0888-8809/02/$15.00/0
Printed in U.S.A.

Molecular Endocrinology 16(4):799–813

Variant Amino Acids in the Extracellular Loops of Murine and Human Vasopressin V2 Receptors Account for Differences in Cell Surface Expression and Ligand Affinity

ALEXANDER OKSCHE, GABRIELE LEDER, SUSANNE VALET, MATTHIAS PLATZER, KERSTIN HASSE, SOEREN GEIST, GERD KRAUSE, ANDRÉ ROSENTHAL, AND WALTER ROSENTHAL

Forschungsinstitut für Molekulare Pharmakologie (A.O., G.L., S.V., K.H., G.K., W.R.), D-13125 Berlin, Germany; Institut für Molekulare Biotechnologie Jena (M.P., S.G., A.R.), 07745 Jena, Germany; Fachhochschule Jena (S.G.), 07745 Jena, Germany; Friedrich-Schiller-Universität (A.R.), Biologisch-Pharmazeutische Fakultät, 07743 Jena, Germany; and Institut für Pharmakologie (W.R.), Freie Universität Berlin, 14195 Berlin, Germany

Cloning and sequencing of the murine chromosomal region XB harboring the murine vasopressin V_2 receptor (mV_2R) gene and comparison with the orthologous human Xq28 region harboring the human vasopressin V_2 receptor (hV_2R) revealed conservation of the genomic organization and a high degree of sequence identity in the V_2R coding regions. Despite an identity of 87% of the amino acid sequences, both receptors show marked functional differences upon stable expression in Chinese hamster ovary cells: the mV_2R displayed a 5-fold higher affinity for [^{3}H]AVP than the human ortholog; similar differences were found for the AVP-mediated activation of adenylyl cyclase. Saturation binding experiments with transiently transfected intact COS.M6 cells showed that the mV_2R was 3- to 5-fold less abundantly expressed at the cell surface than the hV_2R. Laser scanning microscopy of fusion proteins consisting of the V_2Rs and green fluorescent protein (GFP) (mV_2R/GFP, hV_2R/GFP) demonstrated that the hV_2R/GFP was efficiently transported to the plasma membrane, whereas the mV_2R/GFP was localized mainly within the endoplasmic reticulum. Chimeric hV_2Rs, in which the first and/or second extracellular loop(s) were replaced by the corresponding loop(s) of the mV_2R, revealed that the second extracellular loop accounts for the differences in ligand binding, but the first extracellular loop accounts for the reduced cell surface expression. The exchange of lysine 100 by aspartate in the first extracellular loop of hV_2R was sufficient to reduce cell surface expression, which was accompanied by intracellular retention as observed in laser scanning microscopy analysis. Conversely, the exchange of aspartate 100 by lysine in the mV_2R increased the cell surface expression and resulted in predominant plasma membrane localization. Thus, a single amino acid difference in the first extracellular loop between mV_2R and hV_2R determines the efficiency of cell surface expression. (*Molecular Endocrinology* 16: 799–813, 2002)

WATER HOMEOSTASIS IS regulated in most mammals by the neurohypophyseal hormone 8-AVP (8-lysine-vasopressin in swine), acting via the vasopressin V_2 receptor (V_2R) expressed in the principal cells of the renal collecting duct. Cloning and sequencing of the genes encoding the human AVP-neurophysin II precursor (1), the human V_2R [hV_2R (2)] and the human AVP-regulated water-channel aquaporin-2 [AQP2 (3)] enabled elucidation of the origins of congenital forms of diabetes insipidus. Mutations in the AVP-neurophysin II precursor gene (for review see Ref. 4) cause central diabetes insipidus, and mutations in either the V_2R gene or the AQP2 gene are responsible for nephrogenic diabetes insipidus [NDI (5); for review see Ref. 6). More than 150 different mutations (mostly missense and nonsense mutations) of the hV_2R gene (X-linked NDI) and 22 different mutations of the AQP2 gene [21 causing autosomal recessive NDI, one causing autosomal dominant NDI (7)] have been reported.

So far the V_2Rs of man (hV_2R), rat (rV_2R), mouse (mV_2R), cow (bV_2R), pig (pV_2R), and dog (cV_2R) have been cloned (2, 8–10) (GenBank accession nos. AJ006691 and Y18136). Despite amino acid identities of more than 82%, marked interspecies differences

Abbreviations: AQP2, Aquaporin 2; CFP, cyan fluorescent protein; CHO, Chinese hamster ovary; cV2R, hV_2R, mV2R, rV2R, canine, human, murine, and rat- vasopressin V_2 receptor, respectively; DDAVP, 1-deamino-8-D-AVP; endoH, endoglycosidase H; GABA, γ-aminobutyric acid; GFP, green fluorescent protein, HEK, human embryonic kidney, LSM, laser scanning microscopy; MDCK, Madin-Darby canine kidney; NDI, nephrogenic diabetes insipidus; PAC, P1 artificial chromosome; PNGase F, *N*-glycosidase F; RAMP, receptor activity-modifying protein; RXR-motif, arginine/X/arginine-motif; $V_{1A}R$, vasopressin V_{1A} receptor; YFP, yellow fluorescent protein.

have been documented with respect to the affinity to the natural ligand AVP, to the synthetic agonist 1-deamino-8-D-arginine-AVP (DDAVP) (9, 11, 12), and to subtype-specific antagonists (13). These differences represent major obstacles for the development of specific agonists and antagonists that are required for the treatment of polyuria (*e.g*. mutants of V_2R causing partial NDI) or water retention (excess of AVP secretion). Remarkably, the affinities for various different ligands of $mV_{1A}R$ (vasopressin V_{1A} receptor) or $rV_{1A}R$ were almost identical, whereas differences up to 17-fold in antagonist affinities between the rV_2R and the mV_2R have been documented (14). The molecular basis of these differences has not been elucidated. Differences in antagonist affinities have also been noted between rV_2R and hV_2R. These differences were shown to depend on a nonlinear motif, involving one residue of the second (R202 in hV_2R, L202 in rV_2R; R/L202) and one residue of the third extracellular loop (R/G304). However, no differences in the affinities of hV_2R and rV_2R for AVP were noted (13).

Recently, we have cloned and sequenced the complete *L1cam* chromosomal region including the *Avpr2* gene encoding the mV_2R (GenBank accession no. AF133093). The coding regions of the mV_2R and hV_2R are highly homologous: 84% for the nucleotide and 87% for the amino acid sequences. Strikingly, of the 47 variant amino acids (371 amino acids in the mV_2R and hV_2R), 9 are located within the first and second extracellular loops, both of which are known to be crucial for ligand binding (9, 15). In the closely related oxytocin receptor the first and second extracellular loops are identical in seven different species (man, macaque, pig, cow, sheep, mouse, rat). Thus, we speculated that the pharmacological properties of the mV_2R and hV_2R may differ. Comparison of the functional properties of the hV_2R and mV_2R revealed striking species-dependent differences, which are likely to be of physiological relevance. Using chimeric hV_2Rs in which the first and second extracellular loops are replaced either individually or in combination by the corresponding loops of the mV_2R, as well as receptors with single amino acid replacements, we provide evidence that the amino acid residues in the extracellular loops responsible for the high-affinity binding to the mV_2R and the efficient cell surface delivery of the hV_2R are different.

RESULTS

Comparative analysis of the mV_2R gene locus (official gene *Avpr2;* GenBank accession no. AJ0066691) with its human ortholog [official gene *AVPR2* (16); GenBank accession no. U52112] revealed a high degree of conservation: both gene structures and gene orientations are identical, and intron sizes and intergenic distances are closely related.

The open reading frame of the mV_2R gene codes for a 371-amino acid protein (M_r 40,645) which has two consensus sites for *N*-glycosylation, one in the extracellular N terminus (conserved in the rV_2R, hV_2R, pV_2R, bV_2R, and cV_2R), the other in the second extracellular loop (only present in rV_2R and cV_2R; Fig. 1).

Glycosylation of the mV_2R and hV_2R

To analyze the glycosylation pattern of the hV_2R and mV_2R, we expressed both receptors as C-terminal green fluorescent protein (GFP) fusion proteins (hV_2R- and mV_2R/GFP). We recently reported the functional properties (ligand binding and activation of adenylyl cyclase) of the hV_2R/GFP fusion protein to be identical with those of the native hV_2R (17, 18). Similarly, the dissociation constant (K_d) for [^{3}H]AVP and EC_{50} of the AVP-mediated stimulation of adenylyl cyclase by the mV_2R fusion protein were almost identical with those of the native mV_2R (not shown). In Western blot experiments hV_2R/- and mV_2R/GFP proteins were detected with polyclonal anti-GFP antibodies. A broad band at about 75–85 kDa (Fig. 2, indicated by *brackets*) and a strong band at about 60 kDa was found in both cases (Fig. 2, indicated by *arrows*). The bands at about 60 kDa represent the immature, core-glycosylated receptors, as they migrated faster after treatment with endoglycosidase H (endoH; cleaves only high-mannose glycans; Fig. 2, *double arrows*). The broad band (75–85 kDa), which was unaffected by endoH treatment but showed increased mobility after *N*-glycosidase F treatment (PNGaseF; removes both complex and high-mannose glycans) represents mature, complex-glycosylated receptors. In the case of the hV_2R, PNGaseF treatment of the complex-glycosylated hV_2R yielded a protein (Fig. 2, *asterisk*) that migrated slower than either the untreated immature hV_2R or the endoH-treated immature hV_2R. This is explained by the presence of O-linked glycans within the N terminus, which are added in the Golgi apparatus [linked to serine and threonine residues (19)]. In the case of the mV_2R, PNGaseF treatment results mainly in unglycosylated receptor proteins (Fig. 2, mV2R, *double arrows*). In addition, faint immunoreactive bands (Fig. 2, mV2R) migrating more slowly than the unglycosylated receptors were also seen in different immunoblots. These bands may represent low levels of O-glycosylated receptor proteins or incompletely deglycosylated receptor proteins after PNGaseF treatment.

Differences in the Functional Properties of mV_2R and hV_2R

The mV_2R protein differs by only 6 residues from the rV_2R, but by 47 residues from the hV_2R (particularly within the extracellular N terminus, the second extracellular loop, and the intracellular C terminus, Fig. 1). As residues within the extracellular loops of V_{1A}Rs and V_2Rs have been shown to be involved in ligand binding

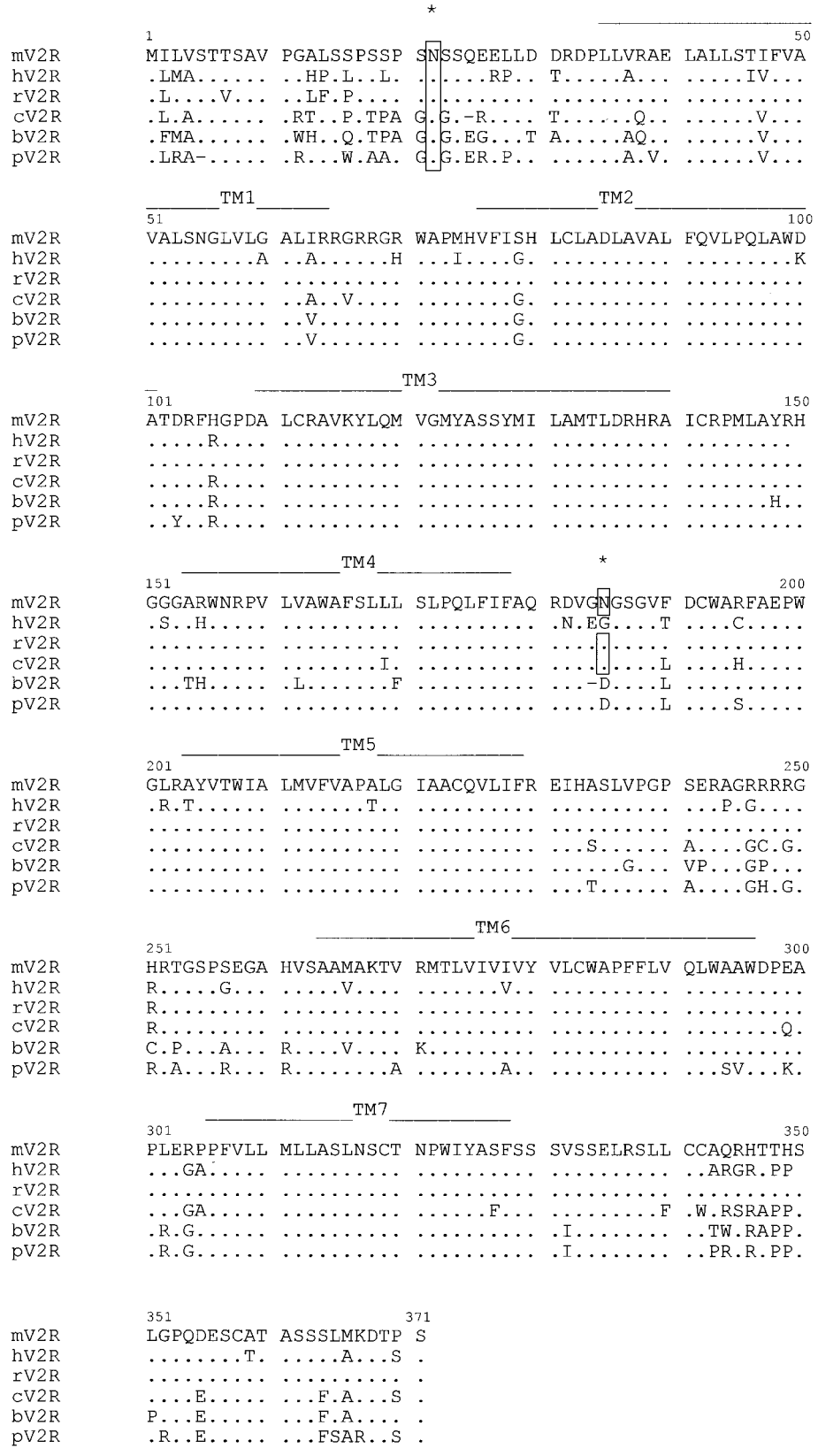

Fig. 1. Amino Acid Alignment of Murine, Human, Rat, Canine, Bovine, and Porcine V_2Rs

The mouse sequence is *capitalized*. Identical amino acids are depicted by *dots*. Exchanges in other species are indicated in *uppercase script* and missing residues by *dashes*. Sites of potential glycosylation (N–X–S/T) are *boxed* and marked by *. Transmembrane domains (TM) 1–7 are indicated. m, Murine; h, human; r, rat; c, canine; b, bovine; p, porcine.

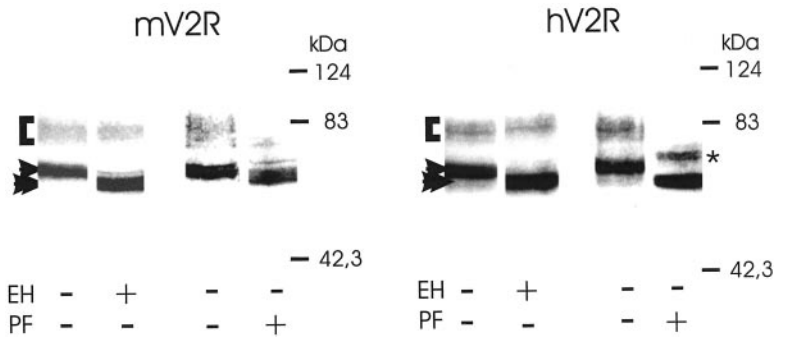

Fig. 2. Immunoblot Analysis of hV_2R/GFP and mV_2R/GFP Fusion Proteins

Fusion proteins were separated on 10% SDS-polyacrylamide gels, transferred onto nitrocellulose filters, and detected with a polyclonal rabbit anti-GFP antibody as first antibody and with a [^{125}I]-labeled antirabbit IgG as second antibody. Untreated or glycosidase-treated membrane proteins (80 μg) from HEK 293 cells transfected with cDNA encoding the hV_2R/GFP or mV_2R/GFP fusion proteins were analyzed. Mock-transfected HEK cells did not reveal any signals (not shown). The positions of the molecular mass standards are indicated. Complex-glycosylated and core-glycosylated V_2Rs are depicted by *brackets* and *arrowheads,* respectively, and their estimated molecular masses are indicated. The *asterisk* indicates the O-glycosylated hV_2R, which became apparent after PNGaseF treatment of the complex-glycosylated receptor protein. In the case of the mV_2R, some faint bands are also seen, which could represent low levels of O-glycosylated receptor proteins or are due to incomplete removal of complex carbohydrates by the PNGaseF treatment. The data are representative of eight separate experiments. PF, PNGaseF; EH, endoH.

(9, 15, 20), we functionally characterized the mV_2R and for comparison the hV_2R, either stably expressed in Chinese hamster ovary (CHO) cells or transiently expressed in COS.M6 or HEK 293 cells, using the natural agonist AVP or the synthetic, selective V_2R agonist DDAVP. In the case of stably expressing cell lines, three independently obtained cell clones were analyzed. The binding capacities ranged from 290–2,100 fmol/mg protein for those clones expressing the hV_2R and from 60–240 fmol/mg protein for those expressing the mV_2R.

[^{3}H]AVP saturation binding analysis to intact CHO cell clones revealed that the mV_2R has an approximately 5-fold higher affinity to the natural ligand than the hV_2R (Tab. 1, Fig. 3, A and B). The synthetic AVP analog DDAVP is known to have an approximately 10 times lower affinity to membrane preparations of human kidney than to those of rat kidney (21). Therefore we investigated the affinity of DDAVP to the mV_2R and the hV_2R in displacement binding experiments with intact CHO cells using [^{3}H]AVP as radioactive ligand (Fig. 3C). Although DDAVP was slightly more potent than AVP in displacing [^{3}H]AVP from the mV_2R, it was about 10-fold less potent in the case of the hV_2R (Table 1 and Fig. 3C). The results confirm data obtained with membrane preparations from human and rat kidney (11, 21).

We also measured the ability of mV_2R and hV_2R to stimulate adenylyl cyclase. To this end, crude membrane preparations of stably transfected CHO cell clones expressing either the mV_2R or the hV_2R were incubated with increasing amounts of the natural agonist AVP or the synthetic agonist DDAVP. Upon treatment with AVP and DDAVP, a saturable activation of adenylyl cyclase activity was observed for membrane preparations of cell clones expressing the mV_2R and hV_2R (Fig. 4). Almost identical EC_{50} values upon treatment with AVP or DDAVP were observed for membrane preparations of mV_2R cell clones (Table 1). In agreement with the displacement analysis, for membrane preparations of hV_2R cell clones, EC_{50} values for AVP-mediated stimulation of adenylyl cyclase were about 5-fold higher than those of mV_2R cell clones; in addition, DDAVP was about 20-fold less potent than AVP in achieving half-maximal activation of adenylyl cyclase (Table 1). Thus, the differences in ligand affinities are reflected by corresponding differences in adenylyl cyclase activation.

We were unable to generate CHO cell clones expressing the mV_2R at levels comparable to those observed for the hV_2R. To eliminate the possible influence of clonal variations on expression levels, we used transiently transfected COS.M6 cells. The dissociation constant (K_d) values were similar to those obtained with stably expressing CHO cell clones (compare Tables 1 and 2). Strikingly, B_{max} values were found to be consistently lower for the mV_2R than for the hV_2R. B_{max} values of at least four separate transfection experiments ranged from 90–150 fmol/mg protein for the mV_2R and from 400–700 fmol/mg protein for the hV_2R (Table 2). Neither transfection of the cells with increasing amounts of cDNA coding for the mV_2R nor variation of DNA/Lipofectin ratios resulted in higher expression levels.

Differences in the Subcellular Distribution of mV_2R/GFP and hV_2R/GFP

To monitor the expression of the receptors more directly, we analyzed the cellular distribution of the mV_2R/GFP and hV_2R/GFP fusion proteins in HEK cells using laser scanning microscopy (LSM). Control cells

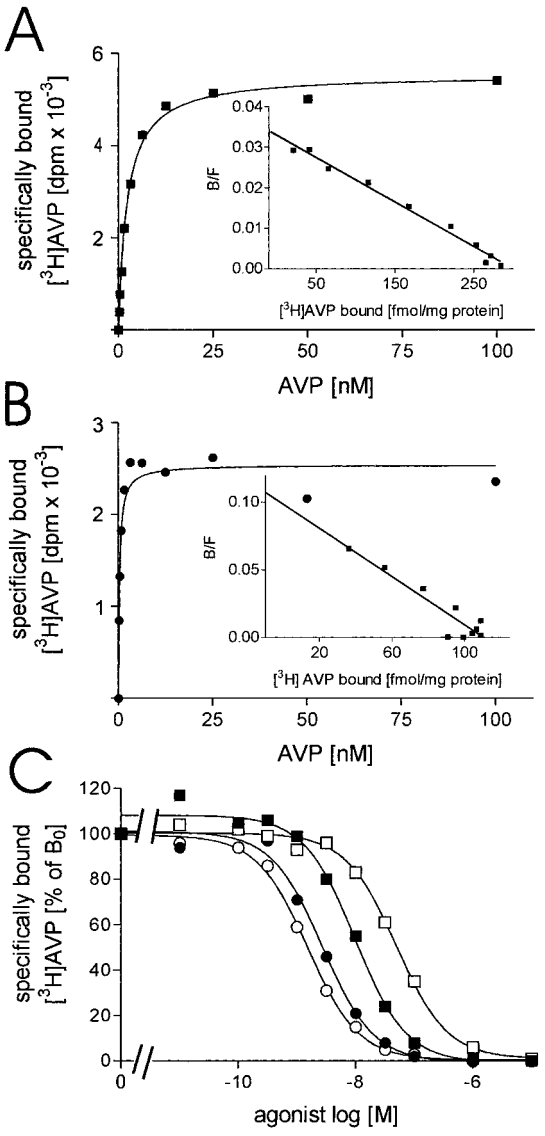

Fig. 3. Saturation and Displacement Binding Analysis of Stably Transfected CHO Cell Clones Expressing the mV_2R or the hV_2R

A and B, [^{3}H]AVP saturation analysis of intact CHO cell clones expressing the hV_2R (A) or the mV_2R (B). Specific (●) binding is indicated. The *inset* shows the Scatchard analysis of specific binding data. Calculated K_d and B_{max} values were 0.35 nM and 108 fmol/mg protein for the mV_2R and 2.5 nM and 296 fmol/mg protein for the hV_2R. Data represent mean values of duplicates which differed by less than 15% and are representative of at least three independent experiments with at least two different cell clones. C, Displacement analysis of [^{3}H]AVP. Intact CHO cells clones expressing the hV_2R (■, □) or the mV_2R (●, ○) were incubated for 2 h with [^{3}H]AVP (2 nM for the hV_2R and 0.7 nM for the mV_2R) and increasing concentrations of AVP (■, ●) or DDAVP (□, ○). Data represent mean values of duplicates which differed by less than 15%. Binding data are depicted as percent of maximal binding for each individual cell clone. Calculated K_i values for AVP and DDAVP were 3.6 nM and 25 nM for hV_2R and 0.96 nM and 0.2 nM for mV_2R, respectively. The data are representative of three to seven separate experiments with at least two different cell clones.

Table 1. Comparison of the Pharmacological Properties of mV_2R and hV_2R Stably Expressed in CHO Cell Clones

	mV_2R (nM)	hV_2R (nM)
K_d [^{3}H]AVP	0.4 ± 0.2	2.2 ± 1.1
K_i AVP	0.8 ± 0.3	2.2 ± 0.8
K_i dDAVP	0.3 ± 0.1	22.5 ± 6.5
EC_{50} AVP	0.6 ± 0.3	3.2 ± 2
EC_{50} dDAVP	0.5 ± 0.2	57 ± 19

Saturation and displacement binding analyses with [^{3}H]AVP as radioligand were performed with intact CHO cell clones expressing either the hV_2R or the mV_2R. K_d and K_i values were calculated from specific binding isotherms using RadLig software. Adenylyl cyclase assays were performed with crude membrane preparations from the respective CHO cell clones. EC_{50} values for the activation of adenylyl cyclase were calculated from concentration-response curves with AVP or DDAVP as agonists. Values are means ± SD of three to five independent experiments, each performed in duplicate.

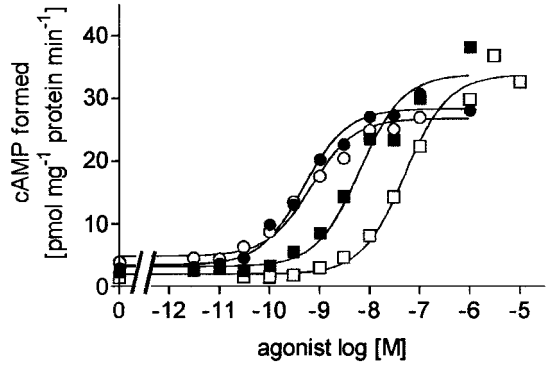

Fig. 4. Adenylyl Cyclase Assays of Membrane Preparations from Stably Transfected CHO Cell Clones Expressing the hV_2R or the mV_2R

Membranes (15–30 μg) derived from CHO cell clones stably expressing the hV_2R (■, □) or the mV_2R (●, ○) were treated with increasing amounts of AVP (■, ●) or DDAVP (□, ○). Values represent mean values of duplicates, which differed by less than 5%. Calculated EC_{50} values for AVP and DDAVP were 5.2 nM and 48 nM for the hV_2R and 0.47 nM and 0.65 nM for the mV_2R, respectively. The data are representative of at least three separate experiments with at least two different cell clones.

were either untransfected or transfected with pEGFP-N1, encoding GFP alone. Whereas in untransfected cells no signals were obtained (Fig. 5A), in those cells transfected with the GFP-encoding plasmid, fluorescent signals were found throughout the cell, including the nucleus (Fig. 5B). This is evident from the signals observed in the horizontal plane (xy-scan, *upper panel*) and the vertical plane (z-scan, *lower panel*) along the indicated *white line*. The mV_2R/GFP protein was present throughout the cell excluding the nucleus (Fig. 5C), and cell surface fluorescence was hardly detectable. In contrast, the hV_2R/GFP protein was mainly found at the plasma membrane, as indicated by a

Table 2. Comparison of K_d and B_{max} Values of Wild-Type mV_2R, hV_2R, and Chimeric hV_2Rs

	K_d (nM)	B_{max} (fmol/mg protein)
hV_2R	3.6 ± 1.9	530 ± 155
mV_2R	0.5 ± 0.1	122 ± 18
HEx1M	2.4 ± 0.2	103 ± 35
HEx2M	1.1 ± 0.1	544 ± 260
HEx1/Ex2M	0.5 ± 0.1	65 ± 21

Saturation binding analyses with [^{3}H]AVP as radioligand were performed with intact COS.M6 cells transiently expressing either the hV_2R, the mV_2R, or chimeric hV_2Rs. HEx1M, HEX2M, and HEx1/Ex2M denote chimeric hV_2Rs in which the first, second, or first and second extracellular loops were replaced by the corresponding murine loop(s), respectively. K_d and B_{max} values were calculated from specific binding isotherms using RadLig software. Values are means ± SD of four to eight independent experiments performed in duplicate.

honeycomb pattern in the xy-scan and a lateral pattern in the z-scan (Fig. 5D). Minor hV_2R/GFP protein signals of variable intensity were also present within the cell (close to the nucleus). These signals could represent transport intermediates on their way to the cell surface or proteins trapped in intracellular membrane compartments as a result of overexpression; however, these signals are clearly different from those observed with the mV_2R/GFP (Fig. 5C).

The hV_2R Is Expressed Mainly at the Cell Surface and the mV_2R Is Located Predominantly Within the Endoplasmic Reticulum

To analyze the subcellular distribution of the V_2Rs in more detail, we used V_2R fusion proteins with spectral variants of GFP [cyan fluorescent protein (CFP); yellow fluorescent protein (YFP)] in conjunction with subcellular localization markers for the plasma membrane (MEM/YFP; CLONTECH Laboratories, Inc., Palo Alto, CA) and the endoplasmic reticulum (ER/CFP; CLONTECH Laboratories, Inc.). The mV_2R/CFP and mV_2R/YFP fusion proteins were predominantly located within the cell (Fig. 6, A and C). The pattern of fluorescence was very similar to that obtained with coexpressed ER/CFP (Fig. 6D) but different from that observed after coexpression with MEM/YFP (Fig. 6B). Thus we conclude that the mV_2R/GFP is predominantly localized within the endoplasmic reticulum and that receptor density at the cell surface is below the detection limit. The distribution of the mV_2R/GFP is in sharp contrast to that of the hV_2R/GFP, which is predominantly found at the plasma membrane, as shown by coexpression with MEM/YFP (Fig. 6, E and F). Coexpression of hV_2R/YFP with ER/CFP confirmed that the hV_2R/GFP is predominantly localized at the plasma membrane (Fig. 6, G and H).

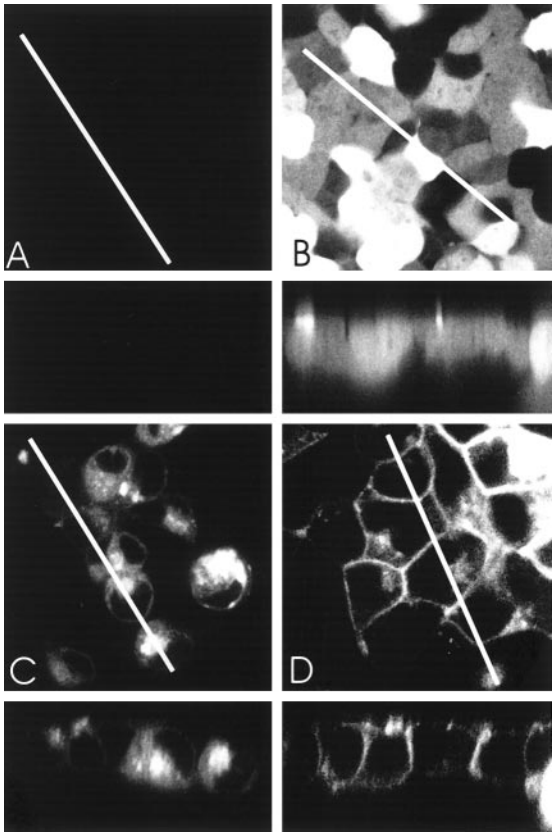

Fig. 5. Localization of mV_2R/GFP and hV2R/GFP Fusion Proteins in Transiently Transfected HEK 293 Cells

HEK 293 cells were transfected with vector pcDNA3 (A), a plasmid encoding GFP alone (B), the mV_2/GFP (C), or the hV_2R/GFP fusion protein (D). Twenty-four hours after transfection the cells were analyzed by LSM. Shown are *horizontal* planes (xy-scan) and corresponding *vertical* planes (z-scans) calculated at the indicated lines from 260 sections (*lower panel*). The data are representative of at least four separate experiments.

Distribution of mV_2R and hV_2R in Madin-Darby Canine Kidney (MDCK) Epithelial Cells

The V_2R is physiologically expressed in polarized principal cells of the renal collecting duct. To exclude the possibility that transport of the mV_2R out of the endoplasmic reticulum to the plasma membrane might be simply impaired in the nonpolarized HEK 293 cells, we transiently expressed both hV_2R/GFP and mV_2R/GFP in polarized MDCK cells. MDCK cells were initially derived from the renal collecting duct of the dog and are widely used for studies of polarized transport. We have recently demonstrated the predominant basolateral expression of hV_2R/GFP fusion proteins in MDCK cells (18, 22). Expression of the mV_2R/GFP, however, resulted in a very similar distribution to that observed in HEK 293 cells, *i.e.* the receptor was predominantly detected intracellularly in xy- and z-scans (Fig. 7, A and D). This was confirmed when the GFP signal was compared with the trypan blue signal (visualization of

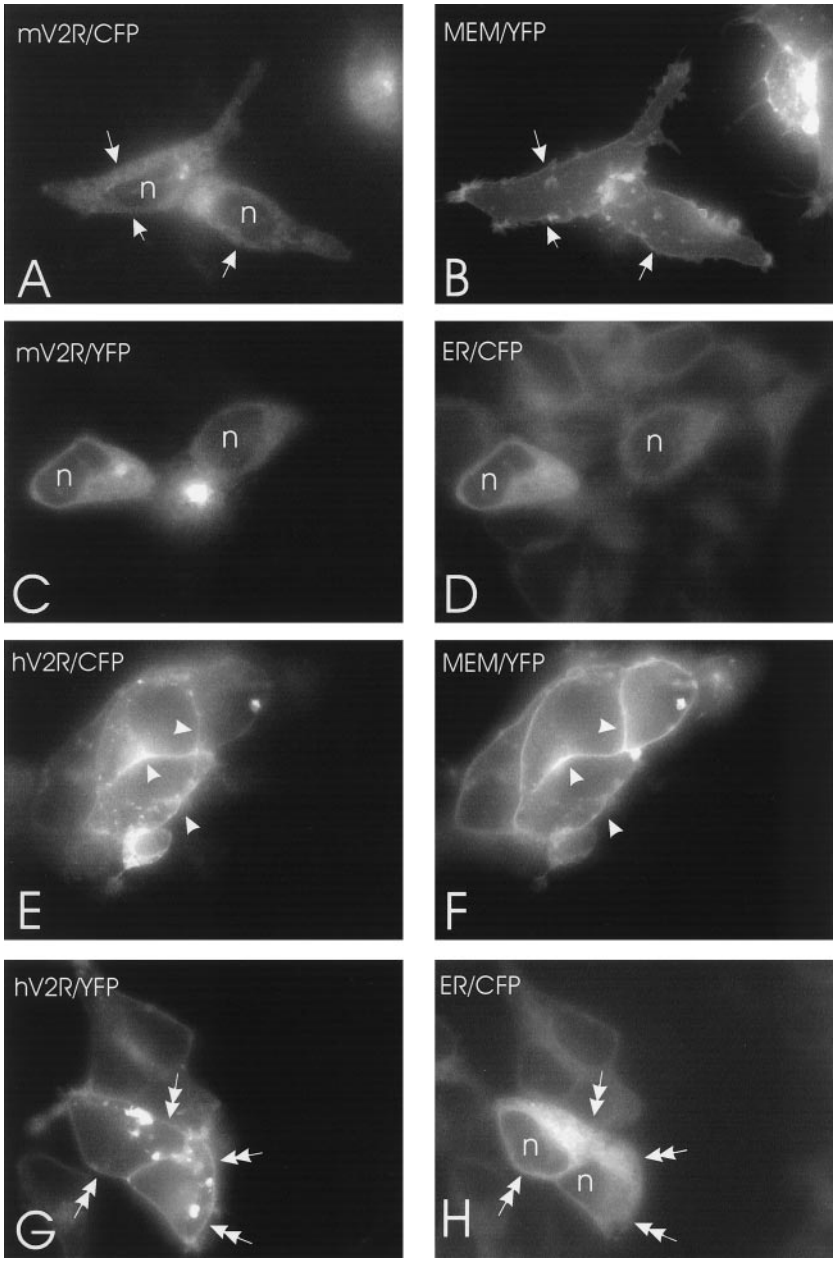

Fig. 6. Subcellular Localization of Spectral Variants of mV_2R/GFP and hV_2R/GFP Fusion Proteins with Organelle-Specific Fusion Proteins

HEK 293 cells were cotransfected with plasmids encoding the mV_2R- or the hV_2R/CFP or/YFP fusion proteins and plasmids encoding a plasma membrane- (MEM/YFP) or endoplasmic reticulum-targeted (ER/CFP) fusion protein. Living cells were analyzed as described in *Materials and Methods*. The expression pattern of the mV_2R/CFP (A) and of MEM/YFP is totally different (B). *Arrows* (A and B) indicate the outline of the plasma membrane as delineated by the MEM/YFP construct. In contrast, expression of the mV_2R/YFP (C) and ER/CFP (D) both reveal the same reticular pattern within the cell, typically of the endoplasmic reticulum. The expression pattern of hV_2R/CFP (E) and of MEM/YFP (F) is very similar. *Arrowheads* indicate the plasma membrane (MEM/YFP, panel F) and show the same outline as found for hV_2R coexpressing cells (E). Coexpression of hV_2R/YFP (G) and ER/CFP (H) confirms that the hV_2R is mainly localized in the plasma membrane (*double arrows*) and not in the endoplasmic reticulum. N, Nucleus.

the plasma membrane; Fig. 7, B and E) or when both signals were overlayed (Fig. 7, C and F). This finding is in contrast to the localization of the hV_2R/GFP (Fig. 7, G and J), which was found almost exclusively at the plasma membrane (see overlays: Fig. 7, I and L).

Significance of Extracellular Loops for the Different Functional Properties of mV_2R and hV_2R

As shown above, the mV_2R is characterized by a high affinity to [^{3}H]AVP but low levels of cell surface

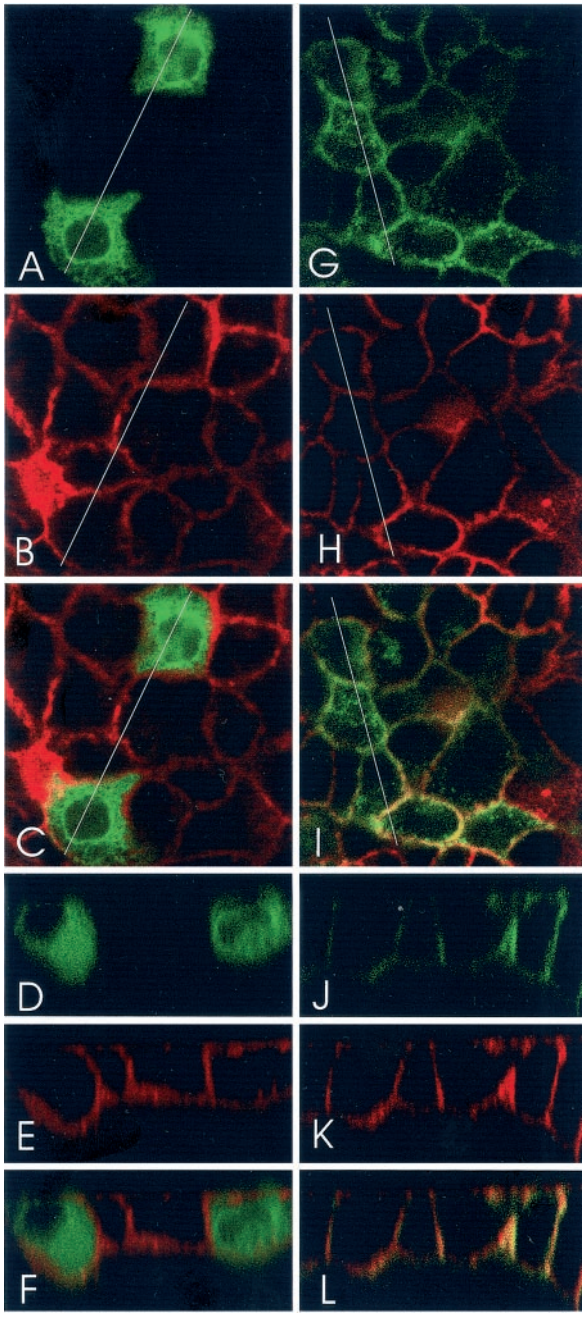

Fig. 7. Localization of mV_2R/GFP and hV2R/GFP Fusion Proteins in Transiently Transfected MDCK Cells

MDCK cells were electroporated with plasmids encoding the mV_2R- (A–F) or the hV_2R/GFP fusion protein (G–L). Twenty-four hours after electroporation the cells were analyzed by LSM for the distribution of the respective receptors. Whereas the mV_2R was found mainly intracellularly in xy- (A) as well as z-scans (D), the hV_2R was found in the plasma membrane in the xy-scan (G) and in z-scans (J). To depict the plasma membranes of MDCK cells, we employed trypan blue staining, which binds to the extracellular part of the membrane of living cells (B and H, xy-scans; E and K, z-scans). An xy-overlay (C) of the fluorescent signals for the mV2R/GFP fusion protein (A) and of the corresponding membrane stain (B) demonstrates the strong intracellular accumulation of the mV_2R. This is also evident in the z-overlay (F). In contrast, the xy-overlay (I) obtained by overlaying fluorescent signals of the hV2R (G) with those of the plasma membrane (H) indicates very similar distributions. This is also shown in the z-overlay (L).

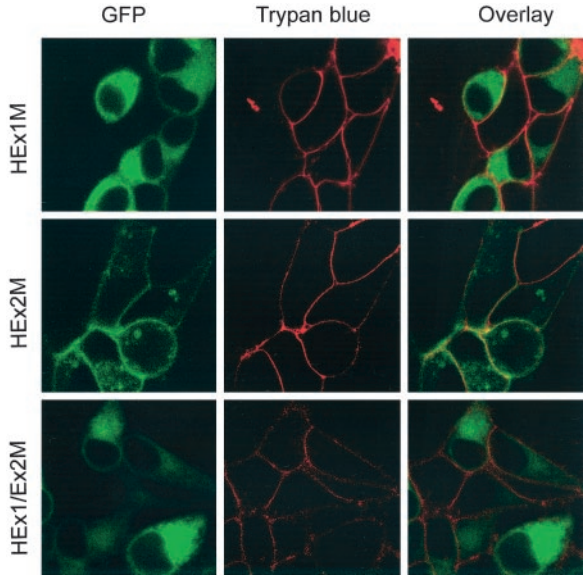

Fig. 8. Localization of the Chimeric HEx1M/GFP, HEx2M/GFP, and HEx1/Ex2M/GFP Fusion Proteins in Transiently Expressing HEK 293 Cells

HEK 293 cells were transfected with plasmids encoding the chimeric hV_2R/GFP proteins harboring the first (HEx1M), the second (HEx2M), or the first and second extracellular loops of the mV_2R (HEx1/Ex2M). Twenty-four hours after transfection the cells were analyzed by LSM. Whereas HEx1M and HEx1/Ex2M were found mainly intracellularly in xy-scans, the HEx2M was predominantly found in the plasma membrane (GFP, *left*). The plasma membranes of HEK cells were stained with trypan blue (trypan blue, *middle*). An overlay of the fluorescence signals (overlay, *right*) obtained for the GFP fusion proteins and the corresponding membrane stain demonstrates plasma membrane localization of the HEx2M, but mainly intracellular retention of the HEx1M and HEx1/Ex2M.

expression compared with the hV_2R. To investigate whether variations in the amino acids of the first and second extracellular loops might account for the difference in affinities, we replaced the first and second extracellular loops of the hV_2R by those of the mV_2R. Three constructs were analyzed, in which either the first (HEx1M), the second (HEx2M), or both loops (HEx1/Ex2M) were exchanged. The constructs were transiently expressed in COS.M6 cells and analyzed by saturation analysis with [^{3}H]AVP. The HEx1M and HEx2M chimeras exhibited an increase in binding affinity compared with the wild-type hV2R (HEx2M displaying lower K_d values than HEx1M; Table 2). The highest receptor affinity, close to that of the mV_2R itself, was achieved when both extracellular loops were replaced (HEx1/Ex2M). A

Table 3. Comparison of K_d and B_{max} Values of hV_2Rs and mV_2Rs Harboring Single Amino Acid Replacements

	K_d (nM)	B_{max} (fmol/mg protein)
hK100D	2.4 ± 0.9	102 ± 31
hR106H	2.4 ± 0.3	590 ± 194
mD100K	0.7 ± 0.3	458 ± 121
mH106R	0.5 ± 0.1	109 ± 25

Saturation binding analyses with [^{3}H]AVP as radioligand were performed with intact COS.M6 cell transiently expressing hK100D, hR106H, mD100K, or the mH106R harboring single amino acid replacements within the first extracellular loop. K_d and B_{max} values were calculated from specific binding isotherms using RadLig software. Values are means ± SD of three to five independent experiments performed in duplicate.

reduced cell surface expression was found for the HEx1M and the HEx1/Ex2M but not for the HEx2M chimeras. In good agreement with the binding data, LSM analyses of HEx2M/GFP revealed a predominant localization within the plasma membrane, whereas the HEx1M/GFP and the HEx1/Ex2M/GFP were mainly located intracellularly (Fig. 8). Thus, the amino acid variations in the first extracellular loop appear to be responsible for differences in cell surface expression.

Intracellular Retention of the mV_2R Is Mediated by a Single Amino Acid in the First Extracellular Loop

The first extracellular loops of the mV_2R and hV_2R differ in two residues: at position 100, an aspartate or lysine residue, and at position 106, a histidine or an arginine residue are found in the mV_2R and hV_2R, respectively. We therefore exchanged these residues in the mV_2R (mD100K, mH106R) and the hV_2R (hK100D, hR106H) to elucidate which variant amino acid(s) in the first extracellular loop determine the differences in cell surface expression. Before functional characterization, we performed fluorescence-activated cell sorting analyses of HEK cells transiently expressing the various GFP fusion proteins. Here very similar transfection efficiencies (varied between 45% and 55%) and almost identical GFP fluorescence intensities were found (data not shown), indicating no gross differences in the transfection efficiencies and the expression rates of the various wild-type and mutant receptors. Saturation binding analysis of transiently transfected COS.M6 cells revealed that the mD100K yielded similar maximal binding capacities as the hV_2R, whereas the binding capacities of the hK100D mutant were almost identical with those of the mV_2R (compare Tables 2 and 3). The mH106R and the hR106H, however, showed no changes in maximal binding capacities when compared with the mV_2R and hV_2R, respectively (compare Tables 2 and 3). The data were supported by LSM analyses of HEK 293 cells

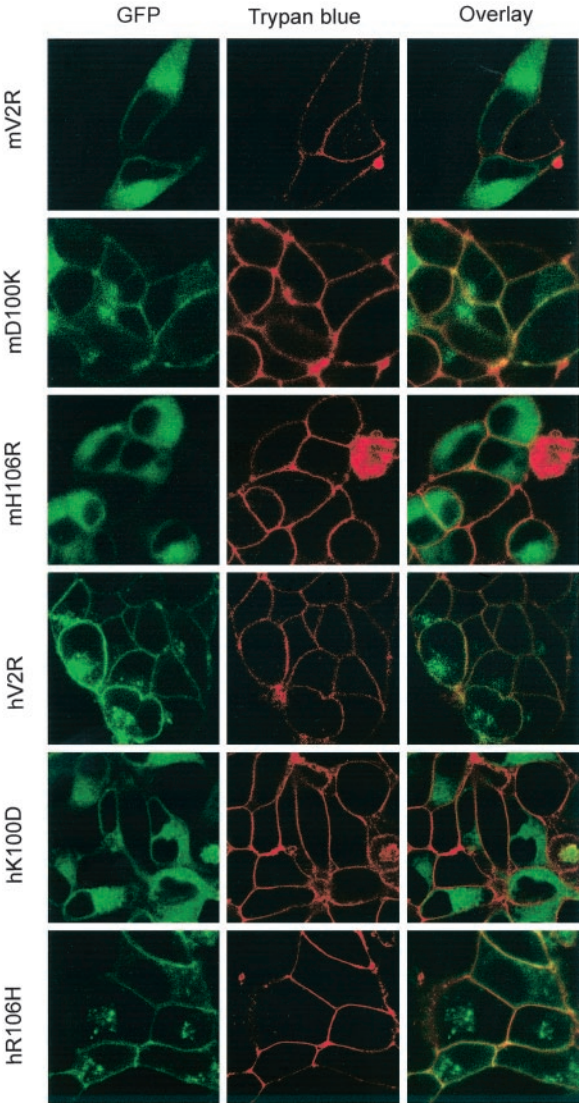

Fig. 9. Localization of Wild-Type And Mutant (Single Amino Acid Replacements) mV_2R/GFP and hV2R/GFP Fusion Proteins in Transiently Expressing HEK 293 Cells

HEK 293 cells were transfected with plasmids encoding the wild-type mV_2R/GFP or hV_2R/GFP or the various mutant mV_2R/GFP and hV_2R/GFP fusion proteins harboring single amino acid replacements in the first extracellular loop. Twenty four hours after transfection the cells were analyzed by LSM. Whereas the mV_2R, mH106R, and hK100D were found mainly intracellularly in xy-scans, the hV_2R, hR106H, and mD100K were predominantly found in the plasma membrane (GFP, *left*). The plasma membranes of HEK cells were stained with trypan blue (trypan blue, *middle*). An overlay of the fluorescent signals (overlay, *right*) ot the GFP fusion proteins and the corresponding membrane stain demonstrates the strong intracellular accumulation of the mV_2R, mH106R, and hK100D, but shows predominant labeling of plasma membranes for the hV_2R, the hR106H, and the mD100K.

transiently expressing the various mutants. The hK100D/GFP mutant was mainly detected within the cell similar to the mV_2R. The counterstain with trypan blue, which visualizes the plasma membrane, further

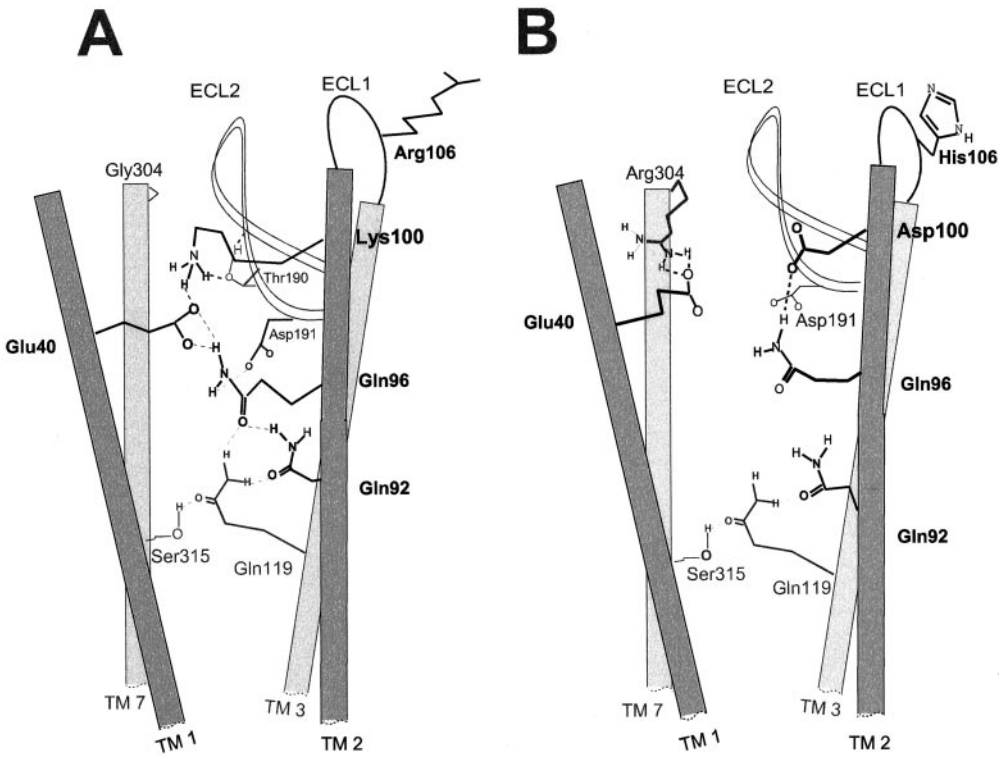

Fig. 10. Scheme of the hV_2R and the mV_2R Depicting the Localization and Molecular Interactions of the Variant Amino Acids 100 and 106 Within the First, Second, and Third Transmembrane Domain and the Second Extracellular Loop

The scheme depicts a computer-assisted homology model of the hV_2R (A) and mV_2R (B) based on the three-dimensional structure published for rhodopsin (Ref. 23; for details see *Materials and Methods*). For clarity only those intramolecular interactions are depicted, which differ between both receptors as a result of the divergent residue 100. Residue 106 is in both models orientated toward the extracellular space and does not show an intramolecular interaction. For further information refer to the text.

supports the predominantly intracellular localization of the hK100D/GFP mutant (Fig. 9). The mD100K/GFP mutant is mainly expressed at the cell surface, which is consistent with the binding data. The fluorescence pattern of the mD100K/GFP is very similar to that of the plasma membrane, as depicted by trypan blue fluorescence. In the case of the mH106R/GFP and the hR106H/GFP mutants, we observed no differences in their subcellular distribution when compared with mV_2R and hV_2R, respectively (Fig. 9).

Our data suggest that the replacement of aspartate 100 by lysine in the mV_2R is sufficient to increase transport out of the endoplasmic reticulum, resulting in higher cell surface expression levels. In the complementary experiment with the hV_2R, the exchange of lysine 100 by aspartate causes retention within the endoplasmic reticulum, which finally leads to a reduction in the cell surface expression levels. This single amino acid residue difference between hV_2R and mV_2R thus readily explains the species-dependent variation in cell surface expression.

Localization of Amino Acids 100 and 106 in a Homology Model of the mV_2R and hV_2R

To gain insight into the potential molecular effects of the variant amino acids at position 100 and 106 that might contribute to the observed differences in cell surface expression, we established a computer-assisted homology model of the hV_2R and mV_2R based on the three-dimensional (3D) structure of rhodopsin (23) (for details of the modeling procedure see *Materials and Methods*). According to this homology model, lysine or aspartate 100 in the hV_2R and mV_2R, respectively, are located at the junction of the second transmembrane domain and the first extracellular loop and are orientated toward the interior region of the receptor. According to our model, the positively charged lysine 100 in the hV_2R is involved in a hydrogen bond network within the upper half of the first, second, and third transmembrane domains and the second extracellular loop (Fig. 10, panel A). This network is formed by the side chains of amino acids lysine 100, glutamate 40, threonine 190, aspartate 191, glutamine 96 and 92, and glutamine 119 and most likely stabilizes the relative orientation of the second transmembrane domain with respect to the first and third transmembrane domain and the second extracellular loop. In the mV_2R, however, the negatively charged aspartate at position 100 most likely disrupts this hydrogen bond network. According to our model, aspartate 100 can interact only with either glutamine 96 and aspartate 191 (Fig. 10, panel B). Moreover, there is no

interaction between glutamate 40 with aspartate 100. In contrast, there is clear repulsion between the three negatively charged residues, aspartate 100, glutamate 40, and aspartate 191. It is possible that this repulsion reorientates glutamate 40 toward arginine 304 found only in the third extracellular loop of the mV_2R (Fig. 10, panel B). In both V_2Rs the amino acid 106 (arginine in hV_2R, histidine in mV_2R) is orientated toward the extracellular space. Based on the rhodopsin structural template, our homology models clearly suggest that lysine/aspartate 100 are involved in intramolecular interactions, whereas arginine/histidine 106 are not. The altered intramolecular interactions, which are caused by the reversed charges of lysine/aspartate 100, might alter slightly the relative orientations of transmembrane helices 1–3. These alterations may provide the molecular basis for the differences in efficient receptor folding and/or cell surface delivery between both V_2Rs. These interpretations are consistent with the experimental data.

DISCUSSION

We show here that mV_2R and hV_2R differ with regard to cell surface delivery and their affinity to the natural ligand AVP, despite high homology of the chromosomal organization of Xq28 and XB and the respective V_2R gene structures and coding regions. The mV_2R displays a 5-fold higher affinity for AVP than the hV_2R. So far, no such difference has been reported for other V_2Rs. By generating chimeric hV_2Rs in which the first and the second extracellular loops were replaced by the corresponding loops of the mV_2R, we were able to confer high-affinity binding to the hV_2R (Table 2). In addition to the differences in ligand binding properties, we observed marked differences in cell surface expression between mV_2R and hV_2R. To our knowledge, such interspecies differences in the cell surface expression of a G protein-coupled receptor (GPCR) have not previously been reported. Earlier reports on differences in the subcellular localization of the subfamily of α_2-adrenergic receptors (α_{2A}, α_{2B}, α_{2C}) were found to be due to the cell system used. Whereas α_{2A} and α_{2B} receptors can be expressed at the cell surface of nonneuronal cells, α_{2C} receptors (naturally present in neurons) are retained within the endoplasmic reticulum. In neuronal PC12 cells, however, α_{2C} receptors are correctly expressed at the cell surface (24). Similar results were obtained with olfactory GPCRs. This family also shows surface expression in neuronal, but not in nonneuronal, cells (25).

We show here that replacement of a positively charged lysine by a negatively charged aspartate at position 100 of the hV_2R (hK100D) causes a dramatic decrease in cell surface delivery (Table 3), accompanied by retention within the endoplasmic reticulum (Fig. 10). In the reverse experiment with a mutant mV_2R, in which aspartate 100 was substituted by lysine (mD100K), a high level of cell surface expression and a distinct plasma membrane localization of the mV_2R were achieved. Several different mechanisms may contribute to the cell surface expression of a protein, including transcriptional, translational, and posttranslational processes. In the case of the mV_2R or the hK100D mutant, the reduced cell surface expression is likely to be due to a posttranslational mechanism, as all receptor proteins were expressed at a comparable level as determined by fluorescence-activated cell sorting analysis (data not shown) but appeared to be retained within the endoplasmic reticulum (see Figs. 6 and 9).

The exit of proteins from the endoplasmic reticulum can be positively or negatively regulated by several mechanisms. Examples are 1) the presence of specific endoplasmic reticulum-retention signals (*e.g*. RXR-based motifs), 2) specific proteins (*e.g*. receptor activity-modifying proteins—RAMPs or Homer proteins), which promote or inhibit receptor trafficking out of the endoplasmic reticulum, or 3) chaperone-mediated retention of misfolded proteins.

RXR-based retention signals inhibit endoplasmic reticulum exit of various proteins, among others the $GABA_{B1}$ receptor. When coexpressed with the $GABA_{B2}$ receptor the RXR motif of the $GABA_{B1}$ receptor is masked by heterodimerization through coiled-coil interactions of the respective C termini, which finally allows transport out of the ER. When the RXR sequence is deleted, the $GABA_{B1}$ receptor (in the absence of $GABA_{B2}$ receptor) is no longer retained within the endoplasmic reticulum but is expressed at the cell surface (26). A similar RXR signal was recently discovered to play a role also in the retention of misfolded hV_2Rs (27). In the case of the calcitonin receptor-like receptor, only its coexpression with RAMPs allows functional cell surface transport of receptors, with distinct ligand selectivities such as the calcitonin gene-related peptide (RAMP1) or adrenomedullin receptors [RAMP2 or RAMP3 28)]. The intracellular trafficking of group I metabotropic glutamate receptors is differentially regulated by Homer proteins; the latter interact with the C termini of glutamate receptors via coiled-coil interactions. Whereas expression of the metabotropic glutamate receptor with Homer 1b results in endoplasmic reticulum retention, expression of the receptors alone or in conjunction with Homer 1a allows efficient delivery to the cell surface (29).

With the exception of RAMP proteins, in which the exact site of interaction with the calcitonin receptor-like receptor has yet not been demonstrated, the signals mediating endoplasmic reticulum retention have been assigned to the cytoplasmic face of membrane proteins. As we could attribute the reduced cell surface expression of the mV_2R to aspartate 100, which is located at the junction of the second transmembrane domain and the first extracellular loop, it is unlikely to function as a specific retention- or transport-promoting signal. It is more likely that the lower levels of cell surface expression of the mV_2R are intrinsic to the receptor protein (*e.g*. receptor folding characteristics)

and not due to the lack of a specific protein promoting export out of the endoplasmic reticulum in the investigated cell lines. This is supported by the finding that saturation binding analysis with membrane preparations from human and murine kidney revealed maximal binding capacities of 700 fmol/mg protein (11) and 29–52 fmol/mg protein, respectively (14, 30). Moreover, female mice, heterozygous for an inactivating mV_2R gene mutation (E242X, a NDI-causing mutation identified in man), show a 3-fold increase in urinary volume and reveal striking concentrating defects when compared with wild-type female mice (urine osmolality is only 50% of that of wild-type female mice). Human females heterozygous for an NDI-causing hV_2R mutant, however, rarely show polyuria or significant concentrating defects. Thus, the relative abundance of the hV_2R in comparison with the mV_2R is also reflected in disease states.

According to the homology model of hV_2R and mV_2R, differences in the intramolecular interactions between transmembrane domain 1, 2, and 3 are likely, which could affect efficient folding. Thus, a major proportion of the newly synthesized mV_2R may not be properly folded. This may favor the binding of chaperones and thereby delay and/or prevent the exit of the mV_2R from the endoplasmic reticulum. A chaperone-mediated endoplasmic reticulum retention was also suggested as a cause of the 20-fold lower cell surface expression in the rat Kv1.1 potassium channel when compared with rat Kv1.4. The endoplasmic reticulum retention of Kv1.1 could be attributed to variant amino acids in the outer pore region and overcome by replacing the outer pore region of Kv1.1 by that of Kv1.4 (31).

Further work will have to confirm the suggested molecular interactions between the first, second, and third transmembrane domain and the second extracellular loop as indicated by the homology model. In addition, it will be intriguing to show whether, indeed, chaperones associate with the mV_2R and thereby cause delayed and/or reduced exit from the endoplasmic reticulum. A possible candidate for further investigations is the chaperone calnexin, which was demonstrated to associate with immature wild-type hV_2R. In addition, calnexin was found to be associated with a disease-causing mutant of the hV2R for prolonged periods when compared with the immature wild-type receptor (32).

The functional differences between mV_2R and hV_2R, despite a high identity of their amino acid sequences, indicates that care must be taken when extrapolating data from animal studies to man.

MATERIALS AND METHODS

Radiochemicals

[^{3}H]AVP (64.8 Ci/mmol), [α-^{32}P]dATP (~30 Ci/mmol), [α-^{32}P]dATP, and [α-^{32}P]dCTP (~3,000 Ci/mmol) were from NEN Life Science Products (Boston, MA).

Chemicals

AVP was synthesized using the solid-phase method (chlorotrityl-resin, 1.05 mmol/g, Calbiochem-Novabiochem GmbH) and purified by HPLC (97% purity). DDAVP and DMEM were purchased from Sigma (Munich, Germany).

Genomic Clones

Two different PAC (P1 artificial chromosome) clones harboring the mouse 129 V_2R gene (GS control number 15528, plate 79; GS control number 15529, plate 93) were purchased from Genome Systems Inc. (St. Louis, MO). The clones were isolated from the Genome Systems P1 129/0La ES cell library (MGSPI) by PCR, using primers corresponding to the hV_2R cDNA sequences (NM 000054) 902–928 (5′-GCC TGC CAG GTG CTC ATC TTC CGG GAG-3′) and 1,179–1,207 (5′-GAT CCA GGG GTT GGT GCA GCT GTT GAG GC-3′) which are highly conserved among the V_2Rs of different species. PACs were propagated and DNA was isolated according to the supplier's protocol.

RT-PCR, Cloning of mV_2R, and the mV_2R/GFP cDNA

Mouse RNA was reverse transcribed into cDNA using the SuperScript Preamplification System (Life Technologies, Inc., Eggenstein, Germany). For subsequent PCR, 4 μl of first-strand cDNA were used as template in a final volume of 50 μl containing 200 μM deoxynucleoside triphosphates, 1.25 U AmpliTaq polymerase, 50 mM KCl, 1.5 mM MgCl, 10 mM Tris/HCl, pH 8.3, 0.01% gelatin (wt/vol), and 200 nM of both sense (5′-ACC ACA CCA TGA TCC TGG TGT CTA CCA CG-3′, corresponding to nucleotides 469–497 of the mouse genomic DNA; GenBank accession no. AJ006691) and antisense primers (5′-GAA AGA GCC CAG TAG CTA CTC AGG AGG G-3′, corresponding to nucleotides 2,099–2,126); start and stop codons are *underlined*. The reaction mixtures were subjected to 30 cycles of 94 C for 30 sec, 60 C for 30 sec, and 72 C for 1 min followed by a final elongation step of 7 min. The PCR fragments were directly subcloned into the pCR2.1 vector, which was transformed into One Shot competent cells (TA Cloning Kit, Invitrogen, Leek, The Netherlands). The resulting plasmid (TA.mV2R) was completely sequenced and was found to carry two silent mutations within codon 131 (TTG instead of CTG) and codon 307 (TTC instead of TTT). In addition, a polymorphism at codon 274 of the mV_2R gene in NMRI mice was found (CTG instead of CTA found in 129 mice). Thereafter, the cDNA was isolated by *Eco*RI digest of the TA.mV2R and cloned into the *Eco*RI-cut and -dephosphorylated pcDNA3 vector (Invitrogen, San Diego, CA). Isolated clones (pmV2R.A3) were verified for the sense orientation of the cDNA, and the complete nucleotide sequence was determined. For the generation of a plasmid encoding the fusion protein of the mV2R and GFP, the termination codon in the pmV2R.A3 was replaced by a *Kpn*I restriction site. To this end, site-directed mutagenesis (Sculptor mutagenesis kit, Stratagene, Heidelberg, Germany) was performed according to the manufacturer's protocol using the forward primer 5′-CAC CCT CCT GGG TAC CTA CTG GG-3′ and the reverse primer 5′-CCC AGT AGG TAC CCA GGA GGG TG-3′ (*Kpn*I restriction site *underlined*). Clones harboring the *Kpn*I site were digested with *Eco*RI/*Kpn*I; the resulting mV_2R cDNA fragment was isolated and cloned into the *Eco*RI/*Kpn*I-digested pEGFP.N1 vector. The integrity of the resulting pmV2R/GFP plasmid was verified by DNA sequencing.

The hV_2R cDNA (comprising the coding region, nucleotides 219–1,354 of the human cDNA sequence, GenBank accession no. 4895106) was isolated from the pRCDN2 plasmid (vector pcDNAI/Neo, 33) by *Xba*I/*Bam*HI digest and subcloned into the *Xba*I/*Bam*HI-cut pCDNA3 vector (phV2R) to produce identical vector constructs for comparative expression analysis.

Site-Directed Mutagenesis

Plasmids encoding single or combined loop replacements of the hV_2R and hV_2R/GFP (HEx1M, HEx2M, HEx1/Ex2M) or single amino acid replacements in the hV_2R and hV_2R/GFP (hK100D, R106H) or the mV_2R and mV_2R/GFP (mD100K, mR106H) were generated with the QuickChange site-directed mutagenesis according to the manufacturer's protocol (Stratagene). All constructs were verified by DNA sequencing.

Sequencing, Assembly, and Comparative Analysis

P1 artificial chromosome DNA preparation and shotgun sequencing were performed as described previously (34). Sequence reactions were electrophoresed on an ABI 377 sequencer. Sequence assembly and manual editing were performed using Staden's GAP4 software (35). The human and mouse sequences were aligned using SIM96 with default parameters (http://globin.cse.psu.edu). Alignment results were plotted with APLOT (http://www1.imim.es/software/gfftools/GFF2.APLOT.html). Alternatively, BLASTZ and the web server Pipmaker (36) were used. In addition, PCR fragments, generated either from a clone harboring the *Eco*RI fragment of the mV_2R gene or directly from the PAC clones and rapid amplification of cDNA ends products, were sequenced with mV_2R-specific primers and the FS Dye Terminator kit (PE Applied Biosystems, Weiterstadt, Germany). The primer sequences are available upon request.

Cell Culture

COS.M6 (kindly provided by Dr. F. Fahrenholz, Frankurt/Main, Germany), HEK 293 (purchased from Deutsche Sammlung für Mikroorganismen und Zellkulturen GmbH, Braunschweig, Germany), and MDCK II cells (kindly provided by Dr. K. Simons, Heidelberg, Germany) were cultured in DMEM. CHO cells (from ATCC, Manassas, VA) were cultured in Ham's F12 and DMEM. All media were supplemented with 10% FCS (PAN Systems GmbH, Nürnberg, Germany), 100 μg/ml streptomycin, and 100 IU/ml penicillin.

Adenylyl Cyclase Assay

The preparation of nuclei-free crude membrane fractions from CHO cells expressing the mV_2R or the hV_2R and the adenylyl cyclase assay were performed as described previously (12). [^{32}P]cAMP was isolated according to the two-column method (37).

Preparation of Membranes from HEK 293 Cells for Immunoblotting

HEK 293 cells grown on 60-mm petri dishes were washed twice with PBS and harvested with a rubber policeman in 0.5 ml PBS supplemented with protease inhibitors (0.5 mM phenylmethylsulfonyl fluoride, 0.5 mM benzamidine, 3.2 μg/ml trypsin inhibitor, 1.4 μg/ml aprotinin). After sonication on ice, membranes and cytosol were separated by ultracentrifugation at 150,000 $\times$ *g* for 1 h. The membranes were washed once with 1 ml PBS, recentrifuged at 150,000 $\times$ *g* for 30 min, resuspended in 80 μl PBS, and stored at -80 C until use.

Immunoblots

Membrane proteins of HEK 293 cells (80 μg per lane) were separated on 10% SDS polyacrylamide gels and transferred onto nitrocellulose filters (Schleicher & Schuell, Dassel, Germany). Protein transfer was monitored by Ponceau red staining. Nitrocellulose filters were blocked with PBS/0.5% Tween 20 (blocking solution), incubated for 1 h with polyclonal rabbit anti-GFP antibody diluted 1:1,000 in PBS/0.05% Tween 20 (washing solution), washed three times, and then incubated for 1 h with [^{125}I]-labeled antirabbit IgG antibody (Amersham Pharmacia LifeScience, Freiburg, Germany) diluted 1:1,000 in washing solution. After three washes, the filter-bound antibodies were exposed to X-OMAT films for 48–72 h. The properties of the polyclonal anti-GFP antibody used in the present study have been described (38).

Generation of Stable Cell Clones and Transient Transfection of Cells

Generation of CHO cell clones stably expressing wild-type mV_2R or hV_2R was performed as described (33).

Transient transfections of COS.M6 and HEK 293 cells were performed using Lipofectin and Lipofectamine, respectively (Life Technologies, Inc.) according to the manufacturer's protocol. In brief, cells were seeded at a density of 50,000 cells per 24-well plate or 1,400,000 cells per 100-mm dish and washed twice the following day with DMEM (containing serum and antibiotics). Mixtures of 0.25 μg DNA/2 μl Lipofectin in 250 μl DMEM, 1 μg DNA/7.5 μl Lipofectin in 1 ml DMEM, and 7 μg DNA/52.5 μl Lipofectin in 2.2 ml DMEM were added to 24-well plates, 35-mm and 100-mm dishes, respectively. The DNA/Lipofectamine mixtures were replaced after 4 h by complete medium, the DNA/Lipofectin mixtures after 16–18 h. The cells were then cultured for an additional 24–48 h.

For the analyses of subcellular localization, cells were cotransfected with plasmids encoding spectral variants (CFP, YFP) of the mV_2R/GFP or hV_2R/GFP fusion proteins and with plasmids encoding subcellular localization markers for the endoplasmic reticulum (pER/CFP, CLONTECH Laboratories, Inc. GmbH, Heidelberg, Germany) and the plasma membrane (pMEM/CFP, CLONTECH Laboratories, Inc. GmbH). Cells grown on coverslips in 35-mm dishes were transfected with a mixture of 0.8 μg DNA of the respective receptor-encoding plasmids (pmV2R/CFP, pmV2R/YFP, phV2R/CFP, and phV2R/YFP) and 0.2 μg DNA of the subcellular localization plasmids (pMEM/YFP, pER/CFP) with 7.5 μl Lipofectamine in 1 ml DMEM.

Transient transfection of MDCK cells was performed by electroporation. To this end, MDCK cell were grown in 60-well dishes overnight and harvested after treatment with trypsin/EDTA. Cells were washed in DMEM, centrifuged at 400 $\times$ *g* for 5 min, and resuspended in DMEM to a final density of 2×10^6 cells/ml. The cell suspension (400 μl) was mixed with 10 μg of plasmid DNA (in 20 μl) and then transferred into a sterile electroporation cuvette. Electroporation was carried out at 280 V, 1,050 microFarads, 481 Ohms for 505 msec. The cell suspension (400 μl) was immediately transferred to 4 ml of DMEM supplemented with 10% FCS; 2.2 ml were plated on 35-mm dishes with coverslips. The cells were analyzed 24–48 h after transfection.

[^{3}H]AVP Binding Analysis

Binding of [^{3}H]AVP to intact COS.M6 cells and CHO cells was essentially as described previously (39). The cells were seeded at a density of 40,000 cells per well in 24-well plates and, in the case of COS.M6 cells, transfected the next day with Lipofectin according to the above mentioned protocol. Two days after plating or transfection of CHO and COS.M6 cells, respectively, 24-well plates were placed on ice and cells were washed twice with ice-cold DPBS (137 mM NaCl; 2.7 mM KCl; 1.5 mM KH_2PO_4; 8.0 mM Na_2HPO_4; 0.9 mM $CaCl_2$; 0.5 mM $MgCl_2$, pH 7.4). For saturation binding analysis the cells were then incubated with increasing concentrations of [^{3}H]AVP diluted in the same buffer in the presence (unspe-

cific binding) or absence (total binding) of 10 μM unlabeled AVP for 2 h on ice. For displacement analysis, cells were incubated with 0.5 or 2 nM [^{3}H]AVP in the presence of increasing concentrations of unlabeled AVP or DDAVP as indicated for 2 h on ice. After washing three times with ice-cold DPBS, the cells were lysed with 0.1 nM NaOH. The lysates were transferred to scintillation vials and radioactivity was determined in a β-counter. K_d and inhibition constant (K_i) values were calculated with RADLIG 4.0 (Biosoft, Cambridge, UK).

LSM

Transiently transfected HEK 293 or MDCK cells grown on glass coverslips were used while subconfluent (24 and 48 h after transfection) or after reaching confluence, respectively. Cells were washed twice with Krebs Ringer HEPES buffer, pH 7.4) and then analyzed on a Carl Zeiss 410 invert laser scanning microscope (Argon/Krypton laser, Carl Zeiss, Jena, Germany). Excitation and emission wave lengths for EGFP were $\lambda_{exc} = 488$ nm and $\lambda_{em} > 515$ nm, respectively.

Fluorescence Microscopy

Transiently transfected HEK 293 cells grown on glass coverslips were washed twice with Krebs Ringer HEPES and mounted on a Carl Zeiss 135 Axiovert microscope. Samples were selectively excited at 440 nm or 485 nm using a polychromatic illumination system (TILL Photonics, Martinsried, Germany), and fluorescence was detected with Omega Filter Set XF88 (Omega Optical Inc., Brattleboro, VT). Images were taken with an Orca (C4742–95) camera (Hamamatsu Photonics, Herrsching, Germany) using Openlab 2.0 software (Improvision, Coventry, UK).

Molecular Modeling

Homology models for mV_2R and hV_2R were built with the Biopolymer module of Sybyl 6.6 (TRIPOS, Inc., St. Louis, MO) using the backbone structure of rhodopsin (24) as a template for the transmembrane and the loop regions. Conformations for insertions in loop regions were taken from similar sequence fragments found in the structural database PDB. For relaxing the side chains, the conformations were minimized and molecular dynamics of 500 psec at 300 K were performed. All calculations were performed using AMBER 5.0 force field as described previously (40).

Acknowledgments

We thank Jenny Eichhorst, Evelyn Michaelis, and Hella Ludewig for technical assistance; Dr. Michael Beyermann and Dagmar Smettan for the synthesis of AVP; Markus Schilhabl for library preparation; Dr. Ralf Schülein for helpful discussion; and John Dickson for reading the manuscript critically.

Received April 23, 2001. Accepted December 7, 2001.

Address all correspondence and requests for reprints to: Alexander Oksche, Forschungsinstitut für Molekulare Pharmakologie, Robert-Rössle-Strasse 10, D-13125 Berlin, Germany. E-mail: oksche@fmp-berlin.de.

This work was supported by the Verbund Klinische Pharmakologie Berlin-Brandenburg, the Fonds der Chemischen Industrie and the German Bundesministerium für Bildung und Forschung (BEO/0311108/0).

REFERENCES

1. Bahnsen U, Oosting P, Swaab DF, Nahke P, Richter D, Schmale H 1992 A missense mutation in the vasopressin-neurophysin precursor gene cosegregates with human autosomal dominant neurohypophyseal diabetes insipidus. EMBO J 11:19–23
2. Birnbaumer M, Seibold A, Gilbert S, Ishido M, Barberis C, Antaramian A, Brabet P, Rosenthal W 1992 Molecular cloning of the receptor for human antidiuretic hormone. Nature 357:333–335
3. Deen PM, Verdijk MA, Knoers NV, Wieringa B, Monnens LA, van Os CH, Van Oost BA 1994 Requirement of human renal water channel aquaporin-2 for vasopressin-dependent concentration of urine. Science 264:92–95
4. Schmale H, Bahnsen U, Richter D 1993 Structure and expression of the vasopressin precursor gene in central diabetes insipidus. Ann NY Acad Sci 689:74–82
5. Arthus MF, Lonergan M, Crumley MJ, Naumova AK, Morin D, De Marco LA, Kaplan BS, Robertson GL, Sasaki S, Morgan K, Bichet DG, Fujiwara TM 2000 Report of 33 novel AVPR2 mutations and analysis of 117 families with X-linked nephrogenic diabetes insipidus. J Am Soc Nephrol 11:1044–1054
6. Oksche A, Rosenthal W 1998 The molecular basis of nephrogenic diabetes insipidus. J Mol Med 76:326–337
7. Mulders SM, Bichet DG, Rijss JP, Kamsteeg EJ, Arthus MF, Lonergan M, Fujiwara M, Morgan K, Leijendekker R, van der Sluijs P, van Os CH, Deen PM 1998 An aquaporin-2 water channel mutant which causes autosomal dominant nephrogenic diabetes insipidus is retained in the Golgi complex. J Clin Invest 102:57–66
8. Lolait SJ, O'Carroll AM, McBride OW, Konig M, Morel A, Brownstein MJ 1992 Cloning and characterization of a vasopressin V2 receptor and possible link to nephrogenic diabetes insipidus. Nature 357:336–339
9. Ufer E, Postina R, Gorbulev V, Fahrenholz F 1995 An extracellular residue determines the agonist specificity of V2 vasopressin receptors. FEBS Lett 362:19–23
10. Gorbulev V, Buchner H, Akhundova A, Fahrenholz F 1993 Molecular cloning and functional characterization of V2 [8-lysine] vasopressin and oxytocin receptors from a pig kidney cell line. Eur J Biochem 215:1–7
11. Guillon G, Butlen D, Cantau B, Barth T, Jard S 1982 Kinetic and pharmacological characterization of vasopressin membrane receptors from human kidney medulla: relation to adenylate cyclase activation. Eur J Pharmacol 85:291–304
12. Birnbaumer M, Hinrichs V, Themmen AP 1990 Development and characterization of a mouse cell line expressing the human V2 vasopressin receptor gene. Mol Endocrinol 4:245–254
13. Cotte N, Balestre MN, Phalipou S, Hibert M, Manning M, Barberis C, Mouillac B 1998 Identification of residues responsible for the selective binding of peptide antagonists and agonists in the V2 vasopressin receptor. J Biol Chem 273:29462–29468
14. Tahara A, Tsukada J, Ishii N, Tomura Y, Wada KI, Kusayama T, Yatsu T, Uchida W, Tanaka A 1999 Characterization of rodent liver and kidney AVP receptors: pharmacologic evidence for species differences. Regul Pept 84:13–19
15. Kojro E, Eich P, Gimpl G, Fahrenholz F 1993 Direct identification of an extracellular agonist binding site in the renal V2 vasopressin receptor. Biochemistry 32: 13537–13544
16. Brenner V, Nyakatura G, Rosenthal A, Platzer M 1997 Compact genomic head to head arrangement of IDH γ and TRAP δ genes in human Xq28 is conserved in rat and mouse. Genomics 44:8–14
17. Oksche A, Dehe M, Schülein R, Wiesner B, Rosenthal W 1998 Folding and cell surface expression of the vaso-

pressin V2 receptor: requirement of the intracellular C-terminus. FEBS Lett 424:57–62
18. Schülein R, Lorenz D, Oksche A, Wiesner B, Hermosilla R, Ebert J, Rosenthal W 1998 Polarized cell surface expression of the green fluorescent protein-tagged vasopressin V2 receptor in Madin-Darby canine kidney cells. FEBS Lett 441:170–176
19. Sadeghi H, Birnbaumer M 1999 O-glycosylation of the V2 vasopressin receptor. Glycobiology 9:731–737
20. Chini B, Mouillac B, Ala Y, Balestre MN, Trumpp-Kallmeyer S, Hoflack J, Elands J, Hibert M, Manning M, Jard S 1995 Tyr115 is the key residue for determining agonist selectivity in the V1a vasopressin receptor. EMBO J 14:2176–2182
21. Butlen D, Guillon G, Rajerison RM, Jard S, Sawyer WH, Manning M 1978 Structural requirements for activation of vasopressin-sensitive adenylate cyclase, hormone binding, and antidiuretic actions: effects of highly potent analogues and competitive inhibitors. Mol Pharmacol 14: 1006–1017
22. Andersen-Beckh B, Dehe M, Schülein R, Wiesner B, Rutz C, Liebenhoff U, Rosenthal W, Oksche A 1999 Polarized expression of the vasopressin V2 receptor in Madin-Darby canine kidney cells. Kidney Int 56:517–527
23. Palczewski K, Kumasaka T, Hori T, Behnke CA, Motoshima H, Fox BA, Le Trong I, Teller DC, Okada T, Stenkamp RE, Yamamoto M, Miyano M 2000 Crystal structure of rhodopsin: a G protein-coupled receptor. Science 289:739–745
24. Hurt CM, Feng FY, Kobilka B 2000 Cell-type specific targeting of the α2c-adrenoceptor. Evidence for the organization of receptor microdomains during neuronal differentiation of PC12 cells. J Biol Chem 275:35424–35431
25. Gimelbrant AA, Haley SL, McClintock TS 2001 Olfactory receptor trafficking involves conserved regulatory steps. J Biol Chem 276:7285–7290
26. Pagano A, Rovelli G, Mosbacher J, Lohmann T, Duthey B, Stauffer D, Ristig D, Schuler V, Meigel I, Lampert C, Stein T, Prezeaui L, Blahos J, Pin J, Froestl W, Kuhn R, Heid J, Kaupmann K, Bettler B 2001 C-terminal interaction is essential for surface trafficking but not for heteromeric assembly of GABA(B) receptors. J Neurosci 21: 1189–1202
27. Hermosilla R, Schülein R 2001 Sorting functions of the individual cytoplasmic domain of the G protein-coupled vasopressin V_2 receptor in Madin-Darby canine kidney epithelial cells. Mol Pharmacol 60:1031–1039
28. McLatchie LM, Fraser NJ, Main MJ, Wise A, Brown J, Thompson N, Solari R, Lee MG, Foord SM 1998 RAMPs regulate the transport and ligand specificity of the calcitonin-receptor-like receptor. Nature 393:333–339
29. Roche KW, Tu JC, Petralia RS, Xiao B, Wenthold RJ, Worley PF 1999 Homer 1b regulates the trafficking of group I metabotropic glutamate receptors. J Biol Chem 274:25953–25957
30. Yun J, Schöneberg T, Liu J, Schulz A, Ecelbarger CA, Promeneur D, Nielsen S, Sheng H, Grinberg A, Deng C, Wess J 2000 Generation and phenotype of mice harboring a nonsense mutation in the vasopressin V2 receptor gene. J Clin Invest 106:1361–1371
31. Zhu J, Watanabe I, Gomez B, Thornhill WB 2001 Determinants involved in Kv1 potassium channel folding in the endoplasmatic reticulum, glycosylation in the Golgi, and cell surface expression. J Biol Chem 276:39419–39427
32. Morello JP, Salahpour A, Petaja-Repo UE, Laperriere A, Lonergan M, Arthus MF, Nabi IR, Bichet DG, Bouvier M 2001 Association of calnexin with wild type and mutant AVPR2 that causes nephrogenic diabetes insipidus. Biochemistry 40:6766–6775
33. Schülein R, Liebenhoff U, Müller H, Birnbaumer M, Rosenthal W 1996 Properties of the human arginine vasopressin V2 receptor after site-directed mutagenesis of its putative palmitoylation site. Biochem J 313:611–616
34. Platzer M, Rotman R, Bauer D, Uziel T, Savitsky K, Bar-Shira A, Gilad S, Shiloh Y, Rosenthal A 1997 Ataxia-telangiectasia locus: sequence analysis of 184 kb of human genomic DNA containing the entire ATM gene. Genome Res 7:592–605
35. Dear S, Staden R 1991 A sequence assembly and editing program for efficient management of large projects. Nucleic Acids Res 19:3907–391135
36. Schwartz S, Zhang Z, Frazer KA, Smit A, Riemer C, Bouck J, Gibbs R, Hardison R, Miller W 2000 PipMaker—a web server for aligning two genomic DNA sequences. Genome Res 10:577–586
37. Salomon Y 1979 Adenylate cyclase assay. Adv Cyclic Nucleotide Res 10:35–55
38. Schülein R, Zühlke K, Oksche A, Hermosilla R, Furkert J, Rosenthal W 2000 The role of conserved extracellular cysteine residues in vasopressin V2 receptor function and properties of two naturally occurring mutant receptors with additional cysteine residues. FEBS Lett 466: 101–106
39. Oksche A, Schülein R, Rutz C, Liebenhoff U, Dickson J, Muller H, Birnbaumer M, Rosenthal W 1996 Vasopressin V2 receptor mutants that cause X-linked nephrogenic diabetes insipidus: analysis of expression, processing and function. Mol Pharmacol 50:820–828
40. Krause G, Hermosilla R, Oksche A, Rutz C, Rosenthal W, Schülein R 2000 Molecular and conformational features of a transport-relevant domain in the C-terminal tail of the vasopressin V2 receptor. Mol Pharmacol 57:232–242